Fabrication and Microscopic and Spectroscopic Characterization of Cytocompatible SelfAssembling Antimicrobial Nanofibers

Dawei Xu¹, Weike Chen², Yuto J. Tobin-Miyaji³, Carolyn R. Sturge⁴, Su Yang², Brendan Elmore¹, Anju Singh⁵, Christine Pybus⁴, David E. Greenberg^{4,6}, Timothy J. Sellati^{*}, Wei Qiang^{3,*}, He Dong^{1, 2,*}

¹Department of Chemistry & Biomolecular Science, Clarkson University, Potsdam, NY, 13699, USA

²Department of Chemistry & Biochemistry, The University of Texas at Arlington, Arlington, TX, 76039, USA

³Department of Chemistry, Binghamton University, SUNY, Binghamton, NY, 13902, USA

⁴Department of Internal Medicine, University of Texas Southwestern Medical Center, Dallas, TX, 75390, USA

⁵Department of Infectious Diseases, Drug Discovery Division, Southern Research Institute, Birmingham, AL, 35255, USA

⁶Department of Microbiology, University of Texas Southwestern Medical Center, Dallas, TX, 75390, USA

E-mail: he.dong@uta.edu, wqiang@binghamton.edu, timsellati@gmail.com

The discovery of AMPs has brought tremendous promise and opportunities to overcome the prevalence of bacterial resistance to commonly used antibiotics. However, their widespread

use and translation into clinical application is hampered by the moderate to severe hemolytic

activity and cytotoxicity. Here we presented and validated a supramolecular platform for the

construction of hemo- and cytocompatible AMP-based nanomaterials, termed Self-Assembling

Antimicrobial Nanofibers (SAANs). SAANs, the "nucleus" of our antimicrobial therapeutic

platform, are supramolecular assemblies of de novo designed AMPs that undergo programmed

self-assembly into nanostructured fibers to "punch holes" in the bacterial membrane, thus killing

the bacterial pathogen. In this study, we performed solid-state NMR spectroscopy showing

predominant antiparallel β-sheet assemblies rather than monomers to interact with liposomes. We

investigated the mode of antimicrobial action of SAANs using transmission electron microscopy

and provided compelling microscopic evidence that self-assembled nanofibers were physically in

contact with bacterial cells causing local membrane deformation and rupture. While effectively

killing bacteria, SAANs, owing to their nanoparticulate nature, were found to cross mammalian

cell membranes harmlessly with greatly reduced membrane accumulation and possess exceptional

cytocompatibility and hemocompatibility compared to natural AMPs. Through these systematic

investigations, we expect to establish this new paradigm for the customized design of SAANs that

will provide exquisite, tunable control of both bactericidal activity and cytocompatibility and can

potentially overcome the drawbacks of traditional AMPs.

KEYWORDS: self-assembly, antimicrobial nanomaterials, peptides, membrane interaction

2

Bacterial resistance to conventional antibiotics has become a major threat to public health and ~\$20 billion in direct medical costs are associated with treatment of antibiotic-resistant infections in the United States each year. 1-3 Most small molecule antibiotics function by penetrating bacteria and acting on specific molecular targets within the pathogen. The ability of bacteria to adapt and evolve their intracellular molecular components, essentially mutating them to circumvent conventional antibiotic treatment, comprises a fundamental strategy underlying development of drug resistance. 4-6 Overuse of the existing antibiotic pipeline has worsened the problem, and as a result, there is an urgent need to develop new types of antimicrobial agents to combat the ever-increasing emergence of multidrug resistant (MDR) bacterial infections.

Host defense peptides (HDPs), also known as antimicrobial peptides (AMPs) are promising candidates that show different mechanisms of action against bacteria. 7-9 AMPs are designed to form amphiphilic structures where hydrophobic and hydrophilic residues segregate to form a binary pattern that interacts with the negatively charged bacterial membrane. The insertion of AMPs into the hydrophobic domain of the lipid membrane leads to membrane pore formation, leakage of cytoplasmic contents and eventually cell death. 7, 10-11 Compared to small molecule antibiotics, AMPs may be less prone to drive the development of antibiotic-resistance since genetic modification of the cell membrane, which AMPs target, is more difficult. Indeed, it has been proven that AMPs can overcome the problem of bacterial resistance. 12-14 Moreover, most AMPs demonstrate broad-spectrum antimicrobial activities owing to their non-specific targeting of cell membranes. 15-17 The AMP structure has inspired the design and synthesis of various antimicrobial polymers as AMP mimetics. 18-21 In particular, a library of quasi-block copolymers was exquisitely demonstrated that showed highly tunable and sequence-controlled antimicrobial and hemolytic activity as commonly observed in natural AMPs. 22

Although AMPs are considered promising alternatives to conventional antibiotics, their widespread use and translation into clinical application is hampered by several intrinsic limitations, including their susceptibility to proteases, short half-lives in circulation, and severe toxicity towards host cells.²³⁻²⁷ Further advancement of the AMP field would greatly benefit from a rational and generic design strategy to overcome AMPs' own intrinsic structural limitations and boost their therapeutic potential.

To enhance AMP-based antimicrobial materials design and potentially overcome the drawbacks of traditional AMPs, peptide assembly has been explored as an effective strategy to fabricate antimicrobial nanomaterials with improved stability and activities. Self-assembled peptide-based bulk hydrogels have been successfully developed by the Schneidar group and several others, which show great promise as injectable tissue scaffolds with intrinsic antimicrobial activities and/or wound dressing. ²⁸⁻³² For solution self-assembly, the Yang group demonstrated a micellar assembly of cholesterol-functionalized cell penetrating peptides that can cross the bloodbrain barrier and suppress bacterial growth in infected brains.³³ The Tirrell group designed AMPfatty acid conjugates and systematically studied their chain-length dependent antimicrobial activity. 34 Most recently, the Gazit group developed a minimalist dipeptide antimicrobial platform and extensively studied the mechanism of the antimicrobial activity of self-assembled peptide nanostructures.³⁵ In addition to peptides, the Boyer and Wong groups reported a novel single chain antimicrobial polymer driven by intrachain folding of a block copolymer that showed high therapeutic indices and good biocompatibility. ³⁶ These studies provide important insights into the fundamental relationship between self-assembly and antimicrobial activity and laid foundation for the emerging area of self-assembled antimicrobial peptides.

Inspired by natural AMP and solution peptide assembly, we recently developed a family of cytocompatible self-assembling antimicrobial nanofibers (SAANs) based on the supramolecular assembly of *de novo* designed multidomain peptides (MDPs). 31, 37-38 MDPs have a general formula of WK_x(QL)_yK_z (amino acid single code letter K: Lysine, Q: Glutamine, L: Leucine, W: Tryptophan) where x, y, z represents the number of the repeating units of each block. Nanofibers are driven by the intermolecular hydrogen bonding and hydrophobic interactions among the (QL) repeating units and their morphology is tuned by the balance of the attractive interaction between the (QL) repeating units and the electrostatic repulsion among the lysine residues. Because of their amphiphilic and cationic nature, these nanofibers were found to display a broad-spectrum antimicrobial activity while having greatly reduced cytotoxicity compared to some of the natural monomeric AMPs. 37

Our central hypothesis is that self-assembly is the key to SAANs' improved cytocompability and bacterial cell selectivity. SAANs differ from conventional monomeric AMPs in that their hydrophobic residues are only partially exposed to the aqueous medium to interact with the hydrophobic domain of the lipid membrane, which could allow control of cell selectivity of SAANs between bacteria and mammalian cells.³⁹⁻⁴¹ In this work, to test the hypothesis and further understand the interplay between self-assembly, antimicrobial activity and cytocompatibility, we performed a detailed spectroscopic and microscopic characterization of SAANs in the context of bacterial cells and phospholipids (to mimic cell membranes). Using solid-state nuclear magnetic resonance (ssNMR) spectroscopy we confirmed the formation of antiparallel β-sheet assemblies of SAANs when in contact with phospholipid bilayers. We demonstrated that local structural flexibility of the terminal leucine residues played important roles in mediating the relative mobility of the peptide subunits within the nanofiber and their

accessibility to interact with the cell membrane. More importantly, the nanofiber-bacteria interaction was directly visualized by TEM showing local membrane damage induced by the nanofiber. These results offered critical structural insights into SAANs and their interaction with the bacterial cell membrane, and greatly improve our fundamental understanding of the mechanistic origin of SAANs' antimicrobial action. We also believe these systematic structural investigations will help further validate the self-assembling platform which can be potentially used for the re-engineering or 're-formatting' of thousands of other natural and synthetic AMPs, thus greatly boosting their therapeutic potential and leveraging investments made by others to combat the expansion of antibiotic resistant pathogens.

RESULTS AND DISCUSSION

Our previous studies showed that MDPs with a proper balance of (QL) repeating units and lysine residues can be formulated into SAANs with tunable cytocompatibility and antimicrobial activity.³⁷ Although the semi-rationale design method based on site-specific residue mutation provided some progress for activity optimization, the mechanistic origin of their antimicrobial activity and mode of membrane interaction remain largely unknown. From materials design point of view, several key questions need to be addressed in order to fully validate this nanostructured platform for antimicrobial therapy and help achieve our overarching goal, namely, SAANs can overcome the intrinsic structural limitations of traditional monomeric AMPs and represent a safer therapeutic delivery modality. These fundamental questions include (1) whether MDPs are assembled when in contact with lipid membranes; (2) how self-assembled peptides interact with and kill bacteria; (3) which critical structural components govern the antimicrobial activity of SAANs; and (4) what is the mechanism for bacterial cell selectivity of action. To address these questions, we chose a MDP that self-assembled into SAANs demonstrating the most potent

antimicrobial activity based on the *in vitro* MIC screening tests. The peptide building block, termed D-W362 (sequence: ${}^{d}W{}^{d}K_{3}(QL)_{6}{}^{d}K_{2}$ in which ${}^{d}W$ and ${}^{d}K$ refer to D amino acids of W and K) consists of mixed L and D amino acids with a central (QL)₆ domain in the L-form flanked by D-lysine residues at both termini. **Figure 1a** shows the chemical structure of the building block and its self-assembly into supramolecular nanofibers.

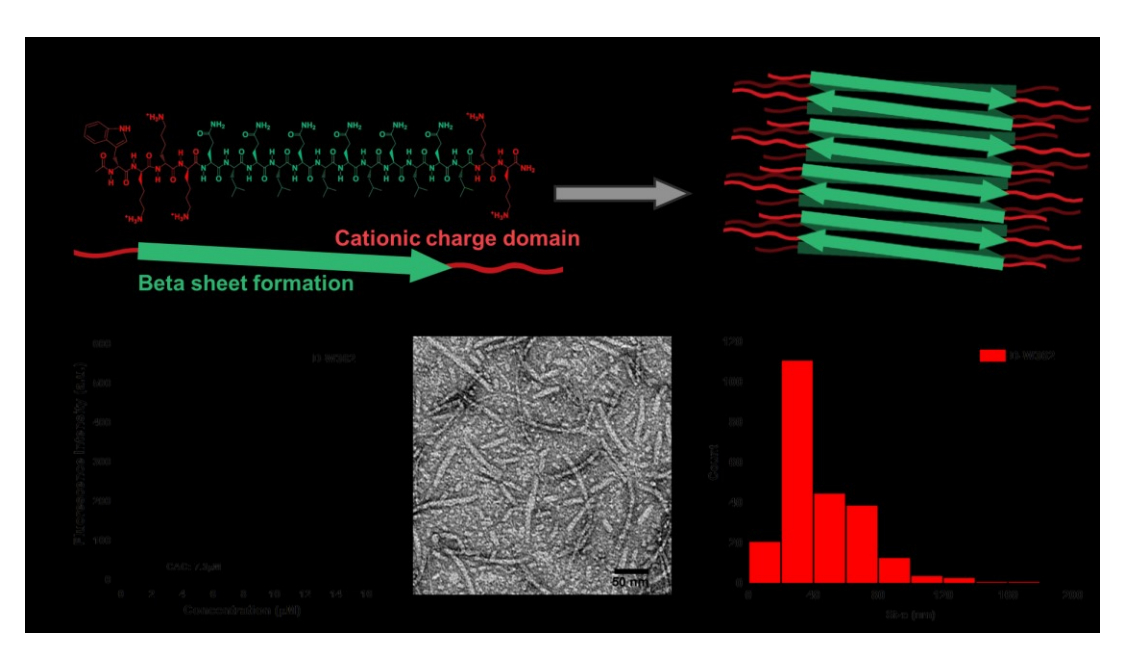


Figure 1. (a) Chemical structure of D-W362 featuring a central β-sheet forming domain of (QL)₆ repeating units (green) and flanking charged lysine residues (red) at the termini and its self-assembly into supramolecular peptide nanofiber. (b) CAC determination by measuring the fluorescence intensity of tryptophan as a function of peptide concentration in Tris buffer (20 mM, pH 7.4). (c) Negatively stained TEM of D-W362 (100 μM in Tris buffer) showing nanofiber formation. (d) Length and length distribution of SAANs formed by D-W362. The result is based on the measurements of 238 nanofibers randomly selected from multiple images.

The ability of D-W362 to assemble was first investigated by critical assembly concentration (CAC) measurement which has been commonly used to evaluate the relative thermodynamic stability of amphiphilic self-assemblies.⁴² D-W362 contains a tryptophan residue which can be used as an intrinsic fluorescence probe to sense the change of polarity around its local environmental as a result of self-assembly.⁴³ Peptide stock solution was prepared by dissolving lyophilized peptide powder in Tris buffer (20 mM, pH=7.4) to reach a final

concentration at 800 µM and left at 4°C for at least two weeks to drive the equilibrium toward the assembled state. For the CAC measurement, the stock solution was diluted to 160 µM and added in proportions of 2 µL each time into 200 µL of Tris buffer to cover a concentration range from 1.6 to 14.5 µM. CACs were determined based on the fluorescence intensity change of tryptophan as a function of peptide concentration (Figure SI-2). At the CAC, fluorescence quenching occurs leading to a deviation of the linear relationship between concentration and intensity. As shown in Figure 1b, a non-linear relationship was observed suggesting the formation of higher ordered assemblies with concentration increases and the CAC was determined to be 7.3 µM. The morphology of self-assembled peptides was visualized by TEM showing nanofibers with an average diameter of ~5 nm and length of ~25 nm (Figure 1c). Our previous study suggested a sandwich-like bilayer \beta-sheet assembly where the leucine residues are buried in the interior and lysine residuals are displayed at the fiber-solvent interface to form a high density of charged surface to interact with the cell membrane.^{37, 44-45} As established in our previous work,³⁸ the nanofiber consists of a double layer of β -sheet packing. The numbers of individual peptides within the nanofiber can be estimated based on the length of a single nanofiber and the spacing between the peptide chains along the fiber long axis which is 4.7 Å as determined by X-ray diffraction for a typical anti-parallel β-sheet secondary structure. Therefore, the total numbers of peptide chains, i.e. the numbers of β-strands in a single fiber to interact with bacteria can be calculated using the formula of (the length of nanofiber in nm /0.47 nm) x 2. Because the nanofiber length is heterogeneous, we will use the average length to calculate the numbers of peptides averaged each nanofiber. Given an average length of 45 nm, we estimate ~ 191 peptide chains within a single fiber.

Gram-negative bacteria are generally more dangerous and much harder to kill than Grampositive bacterial strains due to the presence of a double membrane surrounding bacterial cells. 46-⁴⁸ Therefore, the development of new antimicrobial agents/materials is urgently needed due to the increasing numbers of Gram-negative bacteria that are not responsive to conventional antimicrobial treatments. The antimicrobial activity of D-W362 was evaluated against E. coli by co-incubating peptides with bacteria (100 µL of 1 x 10⁵ CFU/mL) for 18 hrs. The MICs were defined as the minimum peptide concentration at which bacterial growth was completely inhibited and can be estimated by UV absorbance of the bacterial cell culture treated with peptides at different concentrations (2.5 µM to 80 µM). The peptide stock solution prepared for the MIC determination was centrifuged off using a centrifugal filter with a molecular weight cutoff at 30 kDa to remove any residual monomers and oligomers that co-exist with the large assemblies. Using a two-fold serial micro-broth dilution method, the MIC of D-W362 against E. coli was determined to be 20 µM against E. coli, which is higher than its CAC, suggesting self-assembled peptides, rather than monomers, kill the bacteria. The MICs of SAANs were constant after 10 passages of the bacterial culture which was treated with the peptide at half of its MIC value each time while the MIC of penicillin V was dramatically increased (Figure 2). This suggests that SAANs like most conventional AMPs, do not induce drug resistance in E. coli.

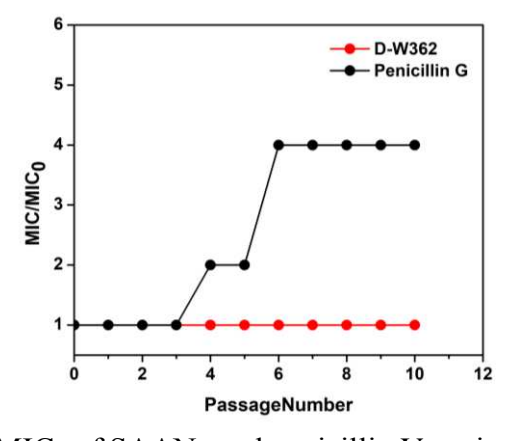


Figure 2. Change of MICs of SAANs and penicillin V against *E. coli* after 10 passages.

The mechanism of antimicrobial activity of SAANs was investigated by confocal laser scanning microscopy (CLSM) and scanning electron microscopy (SEM). **Figure SI-3** shows the results of a live-dead assay wherein *E. coli* cells were incubated with SYTO 9 and Propidium Iodide (PI) in the presence of D-W362 (20 μM) for 60 mins. Live bacteria are indicated by green fluorescence and dead cells by red fluorescence. A significant fraction of *E. coli* cells fluoresced red due to the increased membrane permeability of PI in the presence SAANs that targeted the bacterial membrane. Uptake of rhodamine-dextran (70 kDa) by *E. coli* cells was also observed after 10 mins of incubation in the presence of D-W362 at 20 μM (**Figure 3**). Extended incubation led to enhanced fluorescence as more dextran was taken up by cells. Collectively, these results suggest SAANs' antimicrobial mechanism is to target the bacterial membrane, leading to pore formation, membrane lysis and eventually cell death.

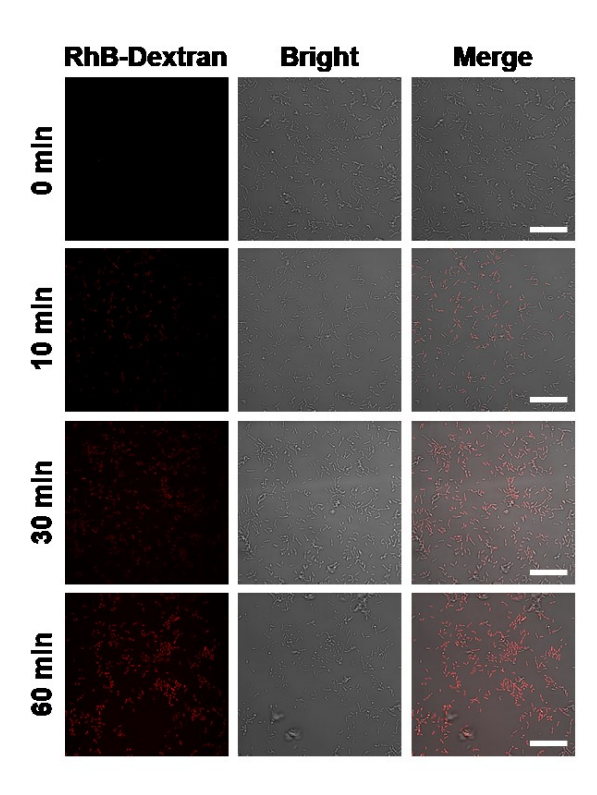


Figure 3. Confocal microscopic images of *E. coli* incubated with rhodamine-labeled dextran (250 mg/L) in the presence of SAANs (20 μ M) for 0 min, 10 min, 30 min and 60 min. Left panel:

fluorescence images of rodamine-dextran. Middle panel: bright field images of bacterial cells; Right panel: merged images. Scale bar: $20 \mu m$.

SEM was used to visualize any morphological changes induced in bacteria by exposure to SAANs. In stark contrast to untreated bacteria (Figure 4a), those incubated with the assembled peptide show significant membrane damage (Figure 4b), suggesting the mode of action is through bacterial membrane disruption. SEM samples underwent several rounds of ethanol dehydration which may potentially degrade peptide nanofibers. To observe both peptides and bacterial cells and understand their physical interaction, we performed negatively stained TEM experiments where peptide-treated bacteria were directly deposited onto a copper grid without further treatment. TEM images shown in Figure 4c (c1 and c2 are high-res images of the nanofibers on the bacterial membrane) confirmed that SAANs directly damage the bacterial cell membrane. TEM of peptidetreated bacteria provided compelling evidence that nanofibers were physically in contact with bacterial cells causing local membrane deformation and rupture, as compared to the control bacterial cells showing relatively more compact and smoother membrane layers (Figure SI-4). To note, TEM experiments were performed multiple times to ensure the images collected were representatives of samples from different cultures to avoid biased results and inaccurate interpretation. Direct visualization of the physical contact between bacterial membrane and nanofibers firmly supports our central hypothesis about the bactericidal activity of SAANs and their mode of action.

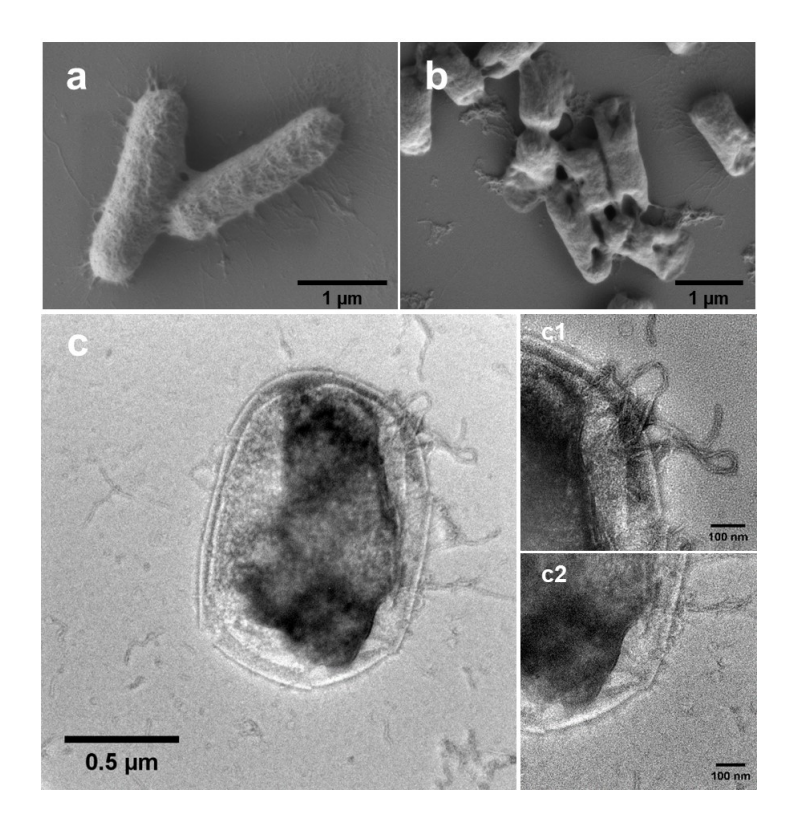


Figure 4. (a) SEM images of control bacteria cells without peptides and (b) upon incubation with D-W362 showing membrane disruption and hole formation. Negatively stained TEM of control bacterial cells without peptide treatment. (c) Bacteria upon incubation with 40 μM of D-W362 showing membrane deformation and rupture. Enlarged images (c1 and c2) showed direct contacts between SAANs and bacterial cells.

The physical interaction between the nanofibers and bacteria was further explored using fluorescence microscopy and proven to be important inbacterial membrane disruption and cell death. This is supported by the observation that co-localization of FITC-labeled nanofibers and dead bacteria as stained with PI was found on a larger fraction of *E. coli* upon peptide treatment. As shown in **Figure SI-5**, 244 bacteria were randomly selected for statistical measurements of the FITC and PI intensity. The autofluorescence intensity of the FITC and PI channel is 500 and 200 for the particular setting used in the experiment. Two defined zones are identified with zone 1 showing the bacteria with only PI staining and zone 2 showing co-localized nanofibers interacting with dead bacteria. Based on the statistical measurement, ~ 85% of dead bacterial cells are attached by nanofibers indicating the important role of physical interaction to cause membrane disruption

and bacterial death. Notably, there are small fractions (~ 15%) of dead cells without peptide attachment, suggesting different mechanisms by which bacteria are killed.

The hemocompatiblity of SAANs was evaluated by incubating human red blood cells (RBCs) with D-W362 at different concentrations for 1 hr and released hemoglobin was measured by UV spectroscopy (Figure SI-6 and Table S1). Within the tested peptide concentrations up to 320 µM (16 times of the MIC) less than 3% of hemolysis was observed with SAANs-treated RBCs compared to the positive control group of RBCs treated with Triton-100, suggesting excellent hemocompatibility and bacterial cell selectivity. More impressively, SAANs were found to harmlessly cross mammalian cell membranes suggesting a greatly reduced capacity to accumulate in the plasma membrane. CLSM was used to identify the cellular localization of FITC-labelled SAANs upon incubation with Bone Marrow Derived Monocytes (BMDMs). The majority of SAANs (shown in green) were found inside BMDMs with minimal staining of the plasma membrane, which remained intact as identified with Texas Red-labelled CD11b (shown in red) after 24 hrs of incubation (Figure 5a). A kinetic study of BMDM cell uptake was performed at various time points for 30 mins, 2 hrs, 6 hrs, and 24 hrs, confirming that nanofibers had minimum accumulation on BMDM membrane at all time points (Figure SI-7). This is in sharp contrast with nanofibers that are localized on bacterial cell membranes causing membrane damage (Figure SI-5). This effect is also different from the cell uptake results seen with a conventional monomeric AMP, Melittin, which resulted in significant damage to and subsequent lysis of the BMDM membrane (Figure 5b). The ability of SAANs to cross the plasma membrane rather than accumulate within it may greatly contribute to reduced cytotoxicity by minimizing membrane disruption, cytosol leakage, and eventual cell death. Although we cannot exclude other

mechanisms, the ability of peptides to assemble may be an important factor for SAANs' membrane selectivity toward bacteria versus mammalian cells.

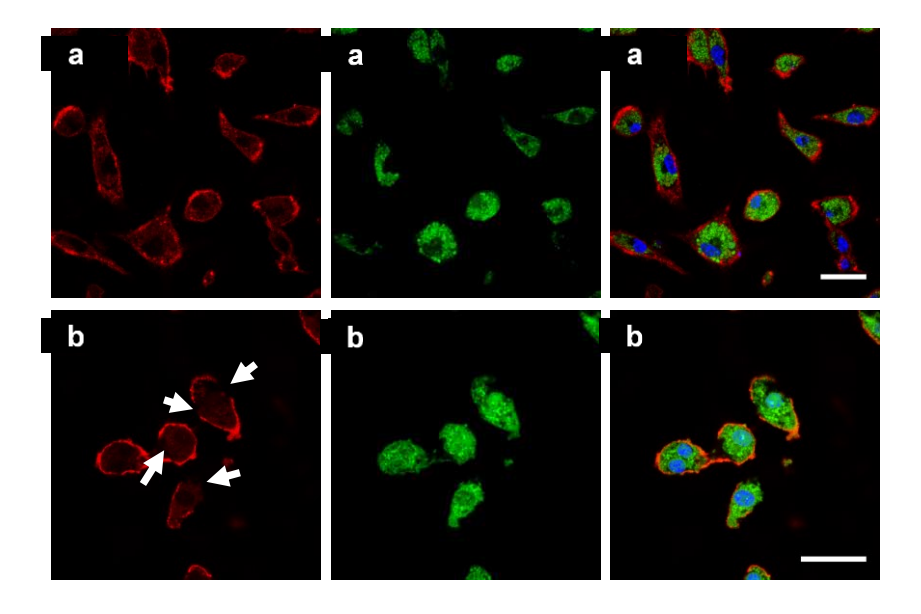


Figure 5. Cellular localization of SAANs monitored by confocal microscopy. BMDMs incubated with (a) FITC-labeled SAANs and (b) FITC-labeled melittin. BMDMs were stained with Texas red-labeled CD11b in red and Hoechst nuclear staining in blue. Left panel: Texas red-labeled CD11b showing BMDMs membrane. Mid panel: FITC-labeled peptides. Right panel: merged images. The arrows on Figure b1 showed significant membrane rupture and damage caused by melittin while SAANs had a minimum effect on membrane integrity. Peptide concentration: 20 μ M. Incubation time: 24 hrs. Scale bar: 20 μ m.

A fundamental question is whether D-W362 maintains its assembled structure or does it dissociate and function as a monomer upon interaction with bacterial cells. Circular dichroism (CD) spectroscopy was employed to monitor the secondary structure of peptide upon mixing with lipid vesicles, which were used to mimic bacterial membranes. The CD sample was prepared by dilution of the aged peptide stock solution to $100 \, \mu M$, followed by the removal of monomers and oligomers using a centrifugal filter with a molecular weight cutoff at 30 kDa. As shown in **Figure S1-8**, D-W362 formed a predominant β -sheet/ β -strand conformation as characterized by the minimum peak at 220 nm when standing alone in aqueous buffer. Upon mixing with lipid vesicles, the secondary structure did not change. However, CD spectroscopy is used to determine the global secondary

structure of peptides and is limited in its ability to differentiate isolated β -strands from assembled β -sheets, neither does it provide local structural information for each individual amino acid. Therefore, high-resolution spectroscopic analysis of SAANs in the context of lipid membranes are highly needed to provide more detailed structural information regarding both the global and local structure of SAANs as well as their assembly states.

Toward this end, we performed ssNMR spectroscopy on samples composed of peptide assemblies associated with phospholipid liposomes at ~1:100 peptide-to-lipid molar ratio through 1D CP, 2D spin diffusion and 13 C-PITHIRDs-CT experiments. $^{49-50}$ These experiments allowed us to answer this fundamental question by determining (1) the local secondary structures of the hydrophobic leucine residues, particularly near the termini and (2) whether peptides form monomers vs. oligomers, parallel vs. antiparallel β -sheet, as well as the registry of the assembly. We first studied the local secondary structures of the four leucine residues close to the termini of the peptide (**Table 1**) by using 1D CP and 2D spin diffusion spectroscopy (to remove the natural abundant lipid signals). For this purpose, four peptides were synthesized containing all 13 C-labeled leucine residues at different sites as shown in **Table 1**.

Table 1. Peptide sequences for 1D CP and 2D spin diffusion NMR spectroscopy studies

Peptide sequences	
	L-N1: WKKKQLQLQLQLQLQL
	L-N2: WKKKQLQLQLQLQLQL KK
	L-C1: WKKKKQLQLQLQLQLQLKKK L-C2: WKKKQLQLQLQLQLQL

(L labeled in red refers to all C13 labeled leucine residues)

As shown in **Figure 6A** and **6B**, the β-strand conformation for all labeled sites was confirmed based on the chemical shift of the ¹³C labeled leucine residues. However, the 2D spectra showed that only the second leucine residue (peptide L-N2 in **Table 1**) from the N-terminus formed a well-

defined β -strand conformation as demonstrated by one clear set of cross-peak for the leucine residue. The other three leucine residues all showed cross peak multiplets on the 2D spectra along with linewidth broadening on the 1D spectra (especially for C_{β}), indicating local structural flexibility of these residues.

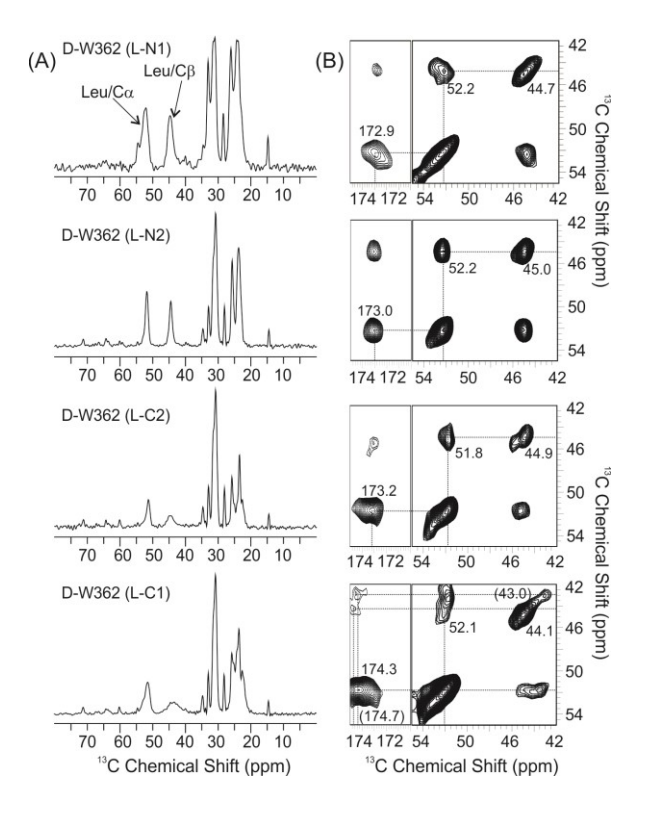


Figure 6. 1D and 2D NMR spectra to probe the local secondary structures. (**A**) 1D 13 C cross polarization spectra for the four Leu-labeled peptide assemblies with membrane bilayers. All spectra were processed with 50 Hz Gaussian line broadening. Leu Cα and Cβ peaks were highlighted in top spectrum. (**B**) 2D 13 C- 13 C spin diffusion spectra for the same samples as in (**A**). All spectra were processed with 50 Hz Gaussian line broadening in both dimensions. Intra-residue cross peaks were highlighted with dashed lines, and the chemical shifts for C', Cα and Cβ were provided. The bottom spectrum contained two sets of cross peaks.

The local flexibility of the leucine residues at both termini play important roles for the antimicrobial activity of SAANs as it may allow partial exposure of these amino acids to the aqueous medium to interact with the lipid membrane and cause membrane disruption and lysis. We next performed ¹³C-PITHIRDs-CT spectroscopy to study and confirm that MDPs interact with lipid membranes in the form of assemblies, rather than monomers. Validation of the assembled

states will help justify our previous assumption that self-assembly is a key factor for SAANs' membrane selectivity. Towards this end, we used D-W362 that were chemically synthesized with singly-¹³C'-labeled Leu residues incorporated in different positions. The labeled residues were shown in **Figure SI-9A**. NMR samples were prepared with either 100% labeled D-W362 (L-N1), or the equivalent mixtures of D-W362 (L-N1) and D-W362 (L-C1). As shown by simulated PITHIRDs decay curves (solid lines in Figure SI-9B, using SIMPSON package),⁵¹ this design allows distinction between non- β -sheet, parallel in-register β -sheet and antiparallel β -sheet structures. The theoretical decay curves were simulated using the ¹³C-¹³C inter-nuclear distances extracted from parallel-in-register and antiparallel structural models in MOLMOL and the appropriate weighing factors (i.e. the cartoon models shown in Figure SI-9C). Comparison between the experimental data (symbols in Figure SI-9B) and theoretical curves clearly supported the formation of an antiparallel β-sheet assembly for D-W362 with the inter-strand hydrogen bonding formed between the amide group of residue i in one chain and the carbonvl group of residue 17-i in the adjacent chain. Taken together, these studies provided solid experimental evidence about the self-assembled states of peptides when in contact with lipid bilayers and validated the supramolecular platform for the fabrication of cytocompatible SAANs. Detailed molecular modeling is also underway through a combined molecular dynamic simulation method and ssNMR spectroscopy using site-specific radio-labeled SAANs and P15 labeled lipids. These studies will help further elucidate the mode of bacterial membrane interaction of SAANs on the atomic level.

In summary, we demonstrated a new way of assembling AMPs leading to antimicrobial nanomaterials with greatly improved stability and cytocompatibility. The formation of the supramolecular nanofiber is the key to improved stability and cytocompatibility of these peptides.

We presented compelling evidence by ssNMR spectroscopy that AMPs (in this case MDPs) are stable in the form of a supramolecular β -sheet assembly when in contact with the lipid membrane. TEM provided direct imaging evidence about the interaction between the nanofiber and bacterial cells and confirmed the antimicrobial mechanism of action of SAANs that target the bacterial cell membrane leading to local membrane deformation and rupture. Owing to their nanoparticulate nature, SAANs demonstrate unique membrane selectivity for bacterial over eukaryotic cells, leading to their greatly enhanced cytocompatibility. We believe this simple yet elegant and effective approach will advance the use of highly cytocompatible AMPs to treat bacterial infections both topically and systemically. Our current efforts coupled with future in vivo studies will afford the field of anti-infective therapy development a unique opportunity to harness the biological properties and functionality of SAANs to combat a wide range of antibiotic-resistant bacterial infections.

MATERIALS AND METHODS

Materials. MBHA rink amide resin, Fluorenylmethyloxycarbonyl (Fmoc)-protected amino acids, 2-(6-Chloro-1-H-benzotriazole-1- yl)-1,1,3,3-tetramethylaminium hexafluorophosphate (HCTU) were purchased from Novabiochem. N,N'-Diisopropylethyl amine (DIPEA), dimethyl formaldehyde (DMF), dichloromethane (DCM), trifluoacetic acid (TFA), triisopropylsilane (TIS) and Tris-HCl buffer (1M, pH=8) (adjusted with 1 M of HCl to pH=7.4) were purchased from Fisher Scientific. Piperidine, α-cyano-4-hydroxycinnamic, rhodamine B-labeled dextran, penicillin V, uranyl acetate and Mueller Hinton Broth (MHB) were from Sigma-Aldrich. DMEM culture medium, Propidium iodide, SYTO 9 stain, phosphate buffered saline (pH=7.4), Texas red labeled CD11b and Hoescht 33342 were purchased from Life Technologies. 1-palmitoyl-2-oleoyl-sn-glycerol-3-phosphocholine (POPC) and 1-palmitoyl-2-oeloyl-sn-glycerol-3-phosphoglycerol

(POPG) were obtained from Avanti Polar Lipids (Alabaster, AL) as dry powders. *Escherichia coli* (*E.coli*) was purchased from ATCC (25922). TEM grids were obtained from Ted Pella (01824). **Minimal inhibitory concentration (MIC) determination.** *E.coli* was cultured in MHB media under constant shaking at 100 rpm at 37 °C to reach their mid-exponential growth phase. The bacterial solution was plated on an agar plate for colony forming unit (CFU) counting. Bacterial suspensions were diluted to approximately 10^5 CFU/mL in MHB media as the initial CFU for inoculation. MIC was estimated based on the 2-fold serial broth microdilution method using peptide concentrations ranging from 25 to 800 μM (three replicates for each concentration). 10μ L of each peptide solution was mixed with 90 μL of bacterial solution in a 96-well plate. The plates were incubated at 37 °C under constant shaking at 100 rpm for 18 hrs and the optical density (OD) at 600 nm was measured. The MIC was determined at the peptide concentration in which OD reading is below 0.06 and no cloudiness was visible to naked eyes.

Mammalian cell uptake. Bone Marrow Derived Monocytes (BMDMs) were used to investigate the cell uptake of SAANs and a natural AMP, Melittin. Bone marrow progenitor cells were isolated from femurs of C57BL/6 mice to enrich for BMDMs as previously described. ^{37, 52} BMDMs were seeded into 35 mm petri dish, 20 mm microwell at a concentration of 1 x 10^5 cells /250 μl /well and allowed to adhere overnight. The following day, cells were treated with 20 μM FITC-labeled peptides and incubated at 37 °C with 5% CO₂ for 24 h. After washing with fresh media, cells were incubated with mixed fluorescent dyes of CD11b (1:200 dilution) and Hoescht 33342 (working concentration 1 μg/ml) in seeding media for 15 min followed by washing and resuspension in fresh media. Images of peptide uptake and localization were captured using a Leica TCS SP5 Laser scanning confocal Microscope operating with the software LAS AF version 2.6.0.7266. Images were acquired using a 63X 1.4NA oil immersion objective. Image processing and analysis was

performed using ImageJ. For the kinetic study of cell uptake, cells were treated with 20 μM FITC-labeled peptides and incubated at 37 °C with 5% CO₂ for 30 mins, 2 hrs, 6 hrs, and 24 hrs. Subsequent washing and staining followed the same procedure as described above. Samples in kinetics experiments, were washed with PBS following staining, fixed in 4% paraformaldehyde for 15 minutes, and stored in PBS at 4 °C protected from light until imaging.

TEM characterization of peptide nanofibers and peptide-treated bacterial cells. TEM was used to analyze peptides and peptide treated bacterial cells. For peptide alone, lyophilized peptide powders were dissolved in Tris buffer (pH=7.4, 20 mM) to reach a final concentration of 100 μ M. 10 μ L of peptide solution was dropped onto a holey carbon grid. After 2 mins, excess solution was carefully removed using a filter paper. The sample was left to dry for 2 mins followed by the addition of 10 μ L of 2 wt% uranyl acetate solution. After 30 secs, excess staining solution was removed and the TEM sample was allowed to dry for at least 8 hrs before imaging. For peptide-treated bacterial cells, 10 μ L of peptide solution (400 μ M) was mixed with 90 μ L of bacterial suspensions (108 CFU/mL). After 8 hrs of incubation at 37 °C, 10 μ L of mixed bacterial suspension was dropped onto a holey carbon grid for 3 mins. Excess solution was removed, and the sample was air-dried for 1 min before staining with 10 μ L of 0.5 wt% uranyl acetate solution. After 3 mins, excess staining solution was removed and the TEM sample was left in air for at least 8 hrs before imaging.

ssNMR spectroscopy. All ssNMR spectra were collected on a 600 MHz Bruker spectrometer equipped with a 2.5 mm TriGamma magic angle spinning (MAS) probe. The NMR samples were prepared by incubating the MDPs in 10 mM Tris-Cl buffer at 80 μM concentration for overnight, followed by mixing with pre-formed lipid vesicles and overnight incubation. The vesicles contained 1-palmitoyl-2-oleoyl-sn-glycerol-3-phosphocholine (POPC) and 1-palmitoyl-2-oeloyl-sn-glycerol-3-phosphocholine (POPC)

sn-glycerol-3-phosphoglycerol (POPG) with a molar ratio 4:1 and the final peptide-to-lipid ratio was set to 1:100. The samples were collected by ultracentrifugation, lyophilized, packed into the 2.5 mm ssNMR rotor, and rehydrated with 5 μ L deionized water. The two-dimensional (2D) spin diffusion spectra were collected with 10 kHz MAS spinning frequency, a 75 kHz 1 H π /2 pulse, 50 kHz 13 C field during the cross polarization, and \sim 100 kHz 1 H decoupling field. The mixing time was set to 20 ms to highlight the intra-residue cross peaks. The 13 C-PITHIRDs-CT spectroscopy was collected with pulse sequences that contained 1 H- 13 C cross polarization (CP) followed by rotor-synchronized 13 C π -pulse train at 50 kHz. The pulsed spin-locking (PSL) acquisition was utilized to enhance the signal-to-noise ratio. The MAS frequencies were set to 10 kHz and 20 kHz for the 2D spin diffusion and 13 C-PITHIRDs-CT experiments, respectively. Sample temperature was controlled using N₂ flow at \sim 278 K based on the monitoring of 1 H chemical shifts of H₂O. The 2D spectra were processed with nmrPipe package and 50 Hz Gaussian line broadening in both dimensions.

ASSOCIATED CONTENT

Supporting Information.

This material is available free of charge via the Internet at http://pubs.acs.org. SI includes additional structural characterization and biological activity evaluation by fluorescence, TEM, confocal microscopy and CD spectroscopy.

AUTHOR INFORMATION

Corresponding Author

he.dong@uta.edu, wqiang@binghamton.edu, timsellati@gmail.com

Author Contributions

The manuscript was written through contributions of all authors. All authors have given approval to the final version of the manuscript.

Notes

The authors declare no competing financial interest.

ACKNOWLEDGMENTS

This study was supported by the National Science Foundation (DMR 1824614 and MRI 0922815) and the start-up funds from the Research Foundation of SUNY. We thank Dr. Cara Boutte for the kind discussion and inputs on nanofiber and bacteria co-localization. We thank Dr. Liping Tang for the kind help on bacterial cell culture experiment, Dr. Kytai T. Nguyen and Nikhil Pandy for the kind discussion about cytocompatibility and hemocompatibility. We acknowledge the technical assistance of Kate Luby-Phelps and the NIH award (1 S10 OD021685-01A1) for the use of Zeiss LSM 880 Airyscan inverted laser scanning confocal microscope.

References

- 1. Lushniak, B. D. (2014) Antibiotic resistance: a public health crisis. *Public Health Rep. 129*, 314-316.
- 2. Rossolini, G. M., Arena, F., Pecile, P., Pollini, S. (2014) Update on the antibiotic resistance crisis. *Curr. Opin. Pharmacol.* 18, 56-60.
- 3. Laxminarayan, R., Duse, A., Wattal, C., Zaidi, A. K., Wertheim, H. F., Sumpradit, N., Vlieghe, E., Hara, G. L., Gould, I. M., Goossens, H., Greko, C., So, A. D., Bigdeli, M., Tomson, G., Woodhouse, W., Ombaka, E., Peralta, A. Q., Qamar, F. N., Mir, F., Kariuki, S., Bhutta, Z. A., Coates, A., Bergstrom, R., Wright, G. D., Brown, E. D., Cars, O. (2013) Antibiotic resistance-the need for global solutions. *Lancet Infect. Dis.* 13, 1057-1098.
- 4. Walsh, C. (2000) Molecular mechanisms that confer antibacterial drug resistance. *Nature* 406, 775-781.
- 5. Sengupta, S., Chattopadhyay, M. K., Grossart, H. P. (2013) The multifaceted roles of antibiotics and antibiotic resistance in nature. *Front. Microbiol.* 4, 47.
- 6. Levy, S. B., Marshall, B. (2004) Antibacterial resistance worldwide: causes, challenges and responses. *Nat. Med. 10*, S122-S129.
- 7. Shai, Y. (1999) Mechanism of the binding, insertion and destabilization of phospholipid bilayer membranes by alpha-helical antimicrobial and cell non-selective membrane-lytic peptides. *Biochim. Biophys. Acta.* 1462, 55-70.
- 8. Zasloff, M. (2002) Antimicrobial peptides of multicellular organisms. *Nature 415*, 389-395.
- 9. Hancock, R. E., Sahl, H. G. (2006) Antimicrobial and host-defense peptides as new anti-infective therapeutic strategies. *Nat. Biotechnol.* 24, 1551-1557.
- 10. Epand, R. M., Vogel, H. J. (1999) Diversity of antimicrobial peptides and their mechanisms of action. *Biochim. Biophys. Acta.* 1462, 11-28.
- 11. Brogden, K. A. (2005) Antimicrobial peptides: pore formers or metabolic inhibitors in bacteria? *Nat. Rev. Microbiol.* 3, 238-250.
- 12. Friedrich, C. L., Rozek, A., Patrzykat, A., Hancock, R. E. (2001) Structure and mechanism of action of an indolicidin peptide derivative with improved activity against gram-positive bacteria. *J. Biol. Chem.* 276, 24015-24022.
- 13. Peschel, A., Sahl, H. G. (2006) The co-evolution of host cationic antimicrobial peptides and microbial resistance. *Nat. Rev. Microbiol.* 4, 529-536.
- 14. Fjell, C. D., Hiss, J. A., Hancock, R. E., Schneider, G. (2011) Designing antimicrobial peptides: form follows function. *Nat. Rev. Drug Discov.* 11, 37-51.
- 15. Fennell, J. F., Shipman, W. H., Cole, L. J. (1968) Antibacterial action of melittin, a polypeptide from bee venom. *Proc. Soc. Exp. Biol. Med. 127*, 707-710.
- 16. Ganz, T. (2003) Defensins: antimicrobial peptides of innate immunity. *Nat. Rev. Immunol.* 3, 710-720.
- 17. Niu, Y., Padhee, S., Wu, H., Bai, G., Harrington, L., Burda, W. N., Shaw, L. N., Cao, C., Cai, J. (2011) Identification of γ -AApeptides with potent and broad-spectrum antimicrobial activity. *Chem. Commun.* 47, 12197-12199.
- 18. Chin, W., Zhong, G., Pu, Q., Yang, C., Lou, W., De Sessions, P. F., Periaswamy, B., Lee, A., Liang, Z. C., Ding, X., Gao, S., Chu, C. W., Bianco, S., Bao, C., Tong, Y. W., Fan, W., Wu, M., Hedrick, J. L., Yang, Y. Y. (2018) A macromolecular approach to eradicate multidrug resistant bacterial infections while mitigating drug resistance onset. *Nat. Commun. 9*, 917.

- 19. Yang, C., Krishnamurthy, S., Liu, J., Liu, S., Lu, X., Coady, D. J., Cheng, W., De Libero, G., Singhal, A., Hedrick, J. L., Yang, Y. Y. (2016) Broad-Spectrum Antimicrobial Star Polycarbonates Functionalized with Mannose for Targeting Bacteria Residing inside Immune Cells. *Adv. Healthc. Mater.* 5, 1272-1281.
- 20. Lienkamp, K., Madkour, A. E., Musante, A., Nelson, C. F., Nusslein, K., Tew, G. N. (2008) Antimicrobial polymers prepared by ROMP with unprecedented selectivity: a molecular construction kit approach. *J. Am. Chem. Soc.* 130, 9836-9843.
- 21. Liu, R., Chen, X., Falk, S. P., Masters, K. S., Weisblum, B., Gellman, S. H. (2015) Nylon-3 polymers active against drug-resistant Candida albicans biofilms. *J. Am. Chem. Soc.* 137, 2183-2186.
- 22. Judzewitsch, P. R., Nguyen, T. K., Shanmugam, S., Wong, E. H. H., Boyer, C. (2018) Towards Sequence-Controlled Antimicrobial Polymers: Effect of Polymer Block Order on Antimicrobial Activity. *Angew. Chem. Int. Ed.* 57, 4559-4564.
- 23. Marr, A. K., Gooderham, W. J., Hancock, R. E. (2006) Antibacterial peptides for therapeutic use: obstacles and realistic outlook. *Curr. Opin. Pharmacol.* 6, 468-472.
- 24. Ulvatne, H., Haukland, H. H., Samuelsen, O., Kramer, M., Vorland, L. H. (2002) Proteases in Escherichia coli and Staphylococcus aureus confer reduced susceptibility to lactoferricin B. *J. Antimicrob. Chemother.* 50, 461-467.
- 25. Schmidtchen, A., Frick, I. M., Andersson, E., Tapper, H., Bjorck, L. (2002) Proteinases of common pathogenic bacteria degrade and inactivate the antibacterial peptide LL-37. *Mol. Microbiol.* 46, 157-168.
- 26. Maher, S., McClean, S. (2006) Investigation of the cytotoxicity of eukaryotic and prokaryotic antimicrobial peptides in intestinal epithelial cells in vitro. *Biochem. Pharmacol.* 71, 1289-1298.
- 27. Liu, P., Davis, P., Liu, H., Krishnan, T. R. (1999) Evaluation of cytotoxicity and absorption enhancing effects of melittin a novel absorption enhancer. *Eur. J. Pharm. Biopharm.* 48, 85-87.
- 28. Salick, D. A., Pochan, D. J., Schneider, J. P. (2009) Design of an Injectable β-Hairpin Peptide Hydrogel That Kills Methicillin-Resistant Staphylococcus aureus. *Adv. Mater.* 21, 4120-4123.
- 29. Veiga, A. S., Sinthuvanich, C., Gaspar, D., Franquelim, H. G., Castanho, M. A. R. B., Schneider, J. P. (2012) Arginine-rich self-assembling peptides as potent antibacterial gels. *Biomaterials* 33, 8907-8916.
- 30. Hughes, M., Debnath, S., Knapp, C. W., Ulijn, R. V. (2013) Antimicrobial properties of enzymatically triggered self-assembling aromatic peptide amphiphiles. *Biomater. Sci. 1*, 1138-1142.
- 31. Jiang, L., Xu, D., Sellati, T. J., Dong, H. (2015) Self-assembly of cationic multidomain peptide hydrogels: supramolecular nanostructure and rheological properties dictate antimicrobial activity. *Nanoscale* 7, 19160-19169.
- 32. Liu, Y., Yang, Y., Wang, C., Zhao, X. (2013) Stimuli-responsive self-assembling peptides made from antibacterial peptides. *Nanoscale 5*, 6413-6421.
- 33. Liu, L., Xu, K., Wang, H., Jeremy Tan, P. K., Fan, W., Venkatraman, S. S., Li, L., Yang, Y.-Y. (2009) Self-assembled cationic peptide nanoparticles as an efficient antimicrobial agent. *Nat. Nanotechnol.* 4, 457.
- 34. Chu-Kung, A. F., Nguyen, R., Bozzelli, K. N., Tirrell, M. (2010) Chain length dependence of antimicrobial peptide–fatty acid conjugate activity. *J. Colloid Interface Sci.* 345, 160-167.

- 35. Schnaider, L., Brahmachari, S., Schmidt, N. W., Mensa, B., Shaham-Niv, S., Bychenko, D., Adler-Abramovich, L., Shimon, L. J. W., Kolusheva, S., DeGrado, W. F., Gazit, E. (2017) Self-assembling dipeptide antibacterial nanostructures with membrane disrupting activity. *Nat. Commun.* 8, 1365.
- 36. Nguyen, T.-K., Lam, S. J., Ho, K. K., Kumar, N., Qiao, G. G., Egan, S., Boyer, C., Wong, E. H. H. (2017) Rational Design of Single-Chain Polymeric Nanoparticles That Kill Planktonic and Biofilm Bacteria. *ACS Infect. Dis.* 3, 237-248.
- 37. Xu, D., Jiang, L., Singh, A., Dustin, D., Yang, M., Liu, L., Lund, R., Sellati, T. J., Dong, H. (2015) Designed supramolecular filamentous peptides: balance of nanostructure, cytotoxicity and antimicrobial activity. *Chem. Commun.* 51, 1289-1292.
- 38. Dong, H., Paramonov, S. E., Aulisa, L., Bakota, E. L., Hartgerink, J. D. (2007) Self-assembly of multidomain peptides: balancing molecular frustration controls conformation and nanostructure. *J. Am. Chem. Soc.* 129, 12468-12472.
- 39. Xiong, M., Lee, M. W., Mansbach, R. A., Song, Z., Bao, Y., Peek, R. M., Yao, C., Chen, L.-F., Ferguson, A. L., Wong, G. C. L., Cheng, J. (2015) Helical antimicrobial polypeptides with radial amphiphilicity. *Proc. Natl. Acad. Sci. U.S.A. 112*, 13155-13160.
- 40. Xiong, M., Bao, Y., Xu, X., Wang, H., Han, Z., Wang, Z., Liu, Y., Huang, S., Song, Z., Chen, J., Peek, R. M., Yin, L., Chen, L.-F., Cheng, J. (2017) Selective killing of Helicobacter pylori with pH-responsive helix—coil conformation transitionable antimicrobial polypeptides. *Proc. Natl. Acad. Sci. U.S.A. 114*, 12675-12680.
- 41. Xiong, M., Han, Z., Song, Z., Yu, J., Ying, H., Yin, L., Cheng, J. (2017) Bacteria Assisted Activation of Antimicrobial Polypeptides by a Random Coil to Helix Transition. *Angew. Chem. Int. Ed. 56*, 10826-10829.
- 42. Priev, A., Zalipsky, S., Cohen, R., Barenholz, Y. (2002) Determination of Critical Micelle Concentration of Lipopolymers and Other Amphiphiles: Comparison of Sound Velocity and Fluorescent Measurements. *Langmuir 18*, 612-617.
- 43. Chen, Y., Barkley, M. D. (1998) Toward understanding tryptophan fluorescence in proteins. *Biochemistry* 37, 9976-9982.
- 44. Yang, M., Xu, D., Jiang, L., Zhang, L., Dustin, D., Lund, R., Liu, L., Dong, H. (2014) Filamentous supramolecular peptide-drug conjugates as highly efficient drug delivery vehicles. *Chem. Commun.* 50, 4827-4830.
- 45. Xu, D., Dustin, D., Jiang, L., Samways, D. S., Dong, H. (2015) Designed filamentous cell penetrating peptides: probing supramolecular structure-dependent membrane activity and transfection efficiency. *Chem. Commun.* 51, 11757-11760.
- 46. Sykes, R. B., Matthew, M. (1976) The beta-lactamases of gram-negative bacteria and their role in resistance to beta-lactam antibiotics. *J. Antimicrob. Chemother.* 2, 115-157.
- 47. Skovbjerg, S., Martner, A., Hynsjo, L., Hessle, C., Olsen, I., Dewhirst, F. E., Tham, W., Wold, A. E. (2010) Gram-positive and gram-negative bacteria induce different patterns of cytokine production in human mononuclear cells irrespective of taxonomic relatedness. *J. Interferon. Cytokine. Res.* 30, 23-32.
- 48. Wellington, E. M., Boxall, A. B., Cross, P., Feil, E. J., Gaze, W. H., Hawkey, P. M., Johnson-Rollings, A. S., Jones, D. L., Lee, N. M., Otten, W., Thomas, C. M., Williams, A. P. (2013) The role of the natural environment in the emergence of antibiotic resistance in gramnegative bacteria. *Lancet Infect. Dis.* 13, 155-165.
- 49. Tycko, R. (2007) Symmetry-based constant-time homonuclear dipolar recoupling in solid state NMR. *J. Chem. Phys.* 126, 064506.

- 50. Morcombe, C. R., Gaponenko, V., Byrd, R. A., Zilm, K. W. (2004) Diluting abundant spins by isotope edited radio frequency field assisted diffusion. *J. Am. Chem. Soc.* 126, 7196-7197.
- 51. Bak, M., Rasmussen, J. T., Nielsen, N. C. (2000) SIMPSON: a general simulation program for solid-state NMR spectroscopy. *J. Magn. Reson.* 147, 296-330.
- 52. Singh, A., Rahman, T., Malik, M., Hickey, A. J., Leifer, C. A., Hazlett, K. R., Sellati, T. J. (2013) Discordant results obtained with Francisella tularensis during in vitro and in vivo immunological studies are attributable to compromised bacterial structural integrity. *PLoS One 8*, e58513.

For Table of Contents Only

